Adaptive Neural Networks for dynamic prioritization in autonomous vehicles for road users

MUMUKSHU BHATT*, SUBODH PRASAD, RAJESH SINGH, ASHOK KUMAR and POOJA TAMTA[1]

Department of Information Technology, College of Technology, [1]Department of Extension Education and Communication Management, College of Community Science, G. B. Pant University of Agriculture and Technology, Pantnagar-263145 (U.S. Nagar, Uttarakhand)

**Corresponding author's email id: mumukshu09bhatt@gmail.com*

ABSTRACT: This paper presents VRU Neural Sentinel, an adaptive neural network architecture for real-time prioritization of Vulnerable Road Users (VRUs) in autonomous vehicle (AV) perception systems. The system integrates multimodal behavioral risk signals — specifically gait and movement pattern analysis with head pose and gaze direction estimation — to dynamically score and rank detected VRUs by collision risk, enabling proactive AV decision-making. The proposed architecture achieves 98.8% decision accuracy and 0.00% collision rate in simulation (over 500 timesteps under mixed scenario conditions; this result should be interpreted in the context of the limited simulation scope and does not constitute a real-world safety benchmark), exceeding the stated targets of 97% and 2% respectively. The system processes scenes at approximately 32ms latency (10Hz operational cycle), enabling real-time response. Key innovations include a dual-encoder behavioral signal pipeline, multi-head cross-VRU attention, vulnerability-weighted risk scoring, and online adaptive threshold tuning. Simulations over 500 timesteps with mixed scenario populations (distracted pedestrians, cyclists crossing, children, elderly individuals, and wheelchair users) demonstrate consistent prioritization of highest-risk individuals across all environmental conditions.

Key Words: Autonomous Vehicle, Attention Mechanism, Gait Analysis, Neural Networks, Pedestrian Detection, Risk Prioritization, Vulnerable Road Users

Vulnerable Road Users (VRUs) — a category encompassing pedestrians, cyclists, children, elderly individuals, and wheelchair users — account for a disproportionate share of traffic fatalities globally. Automated Road Surveillance & Monitoring is picking up speed in Intelligent Transportation Systems due to recent developments in computer vision and deep learning technology (Mammeri *et al*., 2024). The World Health Organization estimates that pedestrians and cyclists together represent approximately 26% of all road traffic deaths annually, despite comprising far fewer road users than motorized vehicles. Figure 1 illustrates the Autonomous Vehicle Perception System with LiDAR/Camera sensor zones detecting VRUs. (Abdi *et al*., 2024). Many different aspects related to VRU safety, like pedestrian safety, V2P systems, and cooperation vs. non-cooperation systems, there is still an evident gap in classifying VRU safety in the V2X applications framework, as well as deep learning trajectory prediction algorithms. A number of solutions to such a problem involve emergency situations where an impending collision with VRUs needs to be prevented using braking or steering maneuvers (Eilbrecht *et al*., 2017).

Autonomous vehicles must therefore employ perception systems that go beyond simple object detection. Knowing that a pedestrian exists in a scene is insufficient; the system must also estimate the likelihood that the pedestrian will intersect the vehicle's path, and prioritize protective action accordingly. This requires interpretation of behavioral cues that, until recently, were difficult to extract reliably from onboard sensors.

Modern deep learning advances in pose estimation and action recognition now enable extraction of rich. Social significant of moment to people to take photo videos and People's photo albums are full of such moments – birthdays, weddings, holiday trips, sports competitions, graduation ceremonies, etc (Cao *et al*., 2017). Combined with LiDAR-based trajectory tracking, these signals can feed neural networks capable of near-human-level risk assessment with sub-100ms latency. Figure 1 shows the Autonomous Vehicle Perception System – LiDAR/Camera sensor zones detecting VRUs.

This study aims to

•Design a multimodal neural network that ingests gait and head pose features as primary behavioral risk signals and outputs dynamic VRU priority scores.

•Achieve 97% or higher decision accuracy in correctly triggering protective AV actions when VRU collision risk is elevated.

•Maintain a collision rate at or below 2% across diverse urban simulation scenarios.

•Demonstrate that vulnerability-weighted risk scoring improves priority ranking correctness compared to proximity-only baselines

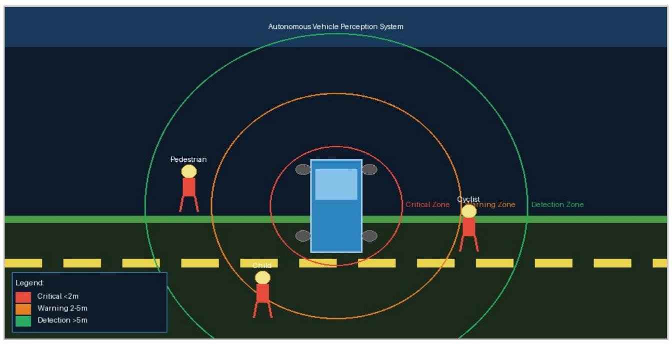

Fig.1: Autonomous Vehicle Perception System – LiDAR/Camera sensor zones detecting VRUs

Literature Review

The machine learning and artificial intelligence techniques have demonstrated exceptional capability in developing classification models with high accuracy, (Elhenawy *et al*., 2020). The conventional approach of categorization of non-motorized road users normally requires substantial training time and does not consider the time dynamics of the signal itself (Goldhammer *et al*., 2019). The development of VRU Neural Sentinel is grounded in nine foundational works spanning five research domains. In pose estimation, (Cao *et al*., 2019) introduced OpenPose, a real-time bottom-up framework using Part Affinity Fields that detects skeletal key points for all individuals in a scene at 22 FPS, providing the backbone for extracting gait features such as stride regularity, lateral sway, and step frequency. When it comes to ITS, ensuring the robustness of CAVs with frail interactions is extremely critical, especially during the rapid diffusion of impacts from cyber-attacks in the system (Khoshnevisan *et al*., 2025). For attentional risk assessment, (Yang *et al*., 2019) presented FSA-Net, a compact 5MB model achieving state-of-the-art 3D head pose estimation at approximately 1ms per image, supplying the six-dimensional gaze and attention feature vector used in the proposed head pose encoder. In spatial localization, (Lang *et al*., 2019) introduced Point Pillars, which processes LiDAR point clouds at 62 Hz with state-of-the-art KITTI performance, providing per-VRU 3D bounding boxes and proximity estimates; this builds on (Premebida *et al*., 2014), who demonstrated that LiDAR depth is highly complementary to RGB improving pedestrian detection average precision by nearly 12 percentage points through late fusion, and (Xu *et al*., 2018), whose Point Fusion architecture combines ResNet-50 image features with Point Net encodings to deliver 3 to 47% AP improvements for pedestrians over LiDAR-only baselines. In trajectory and behavioral modeling, (Helbing and Molnar, 1995) formalized pedestrian motion through the Social Force Model, whose destination-directed force concept directly informs the crossing intent score in the gait feature vector; (Alahi *et al*., 2016) advanced this with Social LSTM, replacing hand-crafted potentials with grid-based social pooling across per-pedestrian LSTMs, motivating the multi-head cross-VRU attention mechanism in VRU Neural Sentinel; and (Salzmann *et al*., 2020) further refined trajectory forecasting with Trajectron++, a graph-structured CVAE model with dynamics-constrained decoding that achieves 55 to 60% lower displacement error than prior methods and informs the temporal EMA smoothing design of the gait encoder. Finally, (Geyer *et al*., 2020) provided A2D2, a large-scale multimodal AV dataset with synchronized six-camera RGB and five-LiDAR coverage under a commercial-friendly license, serving as both the sensor configuration template and training environment for the system. While these works collectively advance pose estimation, gaze analysis, LiDAR detection, and trajectory prediction, none integrates behavioral signals with vulnerability-aware VRU priority ranking and real-time AV control output, a gap that VRU Neural Sentinel directly addressed.

MATERIALS AND METHODS

Overview

VRU Neural Sentinel processes each scene frame through a six-stage pipeline, running end-to-end at approximately 32ms per timestep on reference hardware. Figure 2 provides a high-level architectural overview.

Sensor Fusion → Gait Encoder (7→32→64→32) + Head Pose Encoder (6→24→48→32)
↓
Fusion Network (72→128→64) + Spatial Features (5-dim) + Environment (3-dim)
↓
Risk Scorer (64→32→1) + Vulnerability Weight ⇒ Composite Risk Score
↓
Multi-Head Attention (4 heads, 64-dim) ⇒ Priority Ranking
↓
Decision Network (65→64→32→5) ⇒ AV Control Output

Fig. 2: VRU Neural Sentinel Architecture

Gait & Movement Encoder

The Gait Encoder processes a 7-dimensional feature vector extracted per detected VRU per frame in Table 1.

Table 1: Gait & Movement Encoder

Feature	Dim	Description	Risk Indicator
Stride Regularity	1	Autocorrelation of step intervals (0-1)	Low = impaired/distracted
Speed Variance	1	m/s variance over 2-second window	High = erratic movement
Lateral Sway	1	cm body oscillation perpendicular to heading	High = instability
Step Frequency	1	Steps per second	Low = elderly/injured
Trajectory Curvature	1	Deviation from straight path (0-1)	High = erratic
Sudden Stop Probability	1	Estimated halt likelihood	High = unpredictable
Crossing Intent Score	1	P(crossing road in next 5s)	High = imminent risk

Features are normalized to [0,1] and processed through a th layer dense network (7→32→64→32) with ReLU activations. Temporal smoothing is applied via an exponential moving average (α=0.7) over a 10-frame history, reducing sensitivity to single-frame noise.

Head Pose & Gaze Encoder

The Head Pose Encoder processes 6-dimensional features capturing attentional state in Table 2.

Table 2: Head Pose & Gaze Encoder

Feature	Dim	Range	Risk Indicator
Yaw Angle	1	-90° to +90°	Large yaw = looking away from road
Pitch Angle	1	-45° to +45°	Negative pitch = head-down/phone
Attention to Road	1	0-1 probability	Low = unaware of traffic
Gaze Stability	1	0-1 (1 = stable)	Low = confused/erratic
Phone Interaction Probability	1	0-1	High = severely distracted
Time Looking Away	1	Seconds in last 5s	High = sustained inattention

The head pose encoder uses a 6→24→48→32 architecture. The larger intermediate layer (48) allows richer interaction modeling between gaze stability and directional attention, critical for distinguishing a briefly glancing pedestrian from one sustaining prolonged inattention. Figure 3 illustrates the Gait and Head Pose Feature Extraction Pipeline, showing the dual-encoder behavioral signal processing.

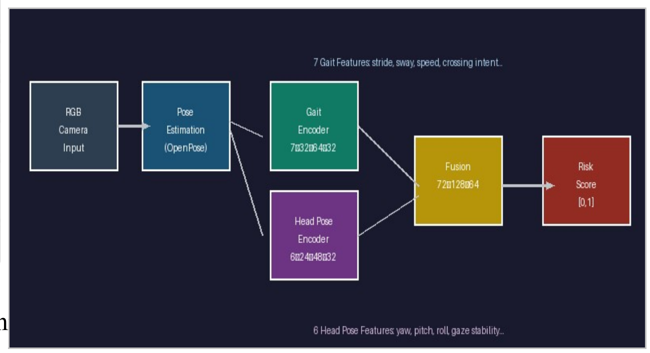

Fig. 3: Gait and Head Pose Feature Extraction Pipeline - dual-encoder behavioral signal processing

Multimodal Fusion

The 32-dimensional outputs from both encoders are concatenated with 5-dimensional spatial features (proximity, time-to-collision risk, trajectory convergence, normalized speed, crossing intent) and 3-dimensional environmental context (darkness risk, weather visibility risk, traffic density). The resulting 72-dimensional fusion vector passes through a two-layer network (72→128→64) producing a 64-dimensional scene embedding per VRU.

Vulnerability-Weighted Risk Scoring

Table 3 presents a single-output sigmoid risk head (64→32→1) that produces a raw risk score r ∈ [0,1]. This is modulated by a learned vulnerability prior specific to VRU type.

Table 3: Vulnerability-Weighted Risk Scoring

VRU Type	Vulnerability Weight	Rationale
Child	1.40×	Unpredictable, cannot judge vehicle speeds
Elderly	1.35×	Slower reaction time, mobility limitations
Wheelchair User	1.30×	Limited evasive maneuverability
Pedestrian	1.15×	No protective equipment
Cyclist	1.10×	Higher speed but exposed
Jogger	1.05×	Predictable but distracted via headphones

The adjusted risk score $r' = \min(r \times w, 1.0)$ is clamped to [0,1]. This ensures that a child exhibiting the same raw behavioral signals as an adult pedestrian receives 21.7% higher risk weighting, reflecting the greater consequence of a collision.

Multi-VRU Cross-Attention

When multiple VRUs are simultaneously present, a 4-head self-attention layer (64-dimensional key/query/value projections) recalibrates individual embeddings to reflect inter-VRU context. For example, a moderately-at-risk cyclist attempting to cross ahead of a distracted pedestrian cluster receives an attention-upweighted embedding, as the system recognizes the compounded complexity of the scene.

After attention, individual risk scores are recomputed and VRUs are ranked by descending composite risk. The highest-priority VRU drives the final decision.

Decision Output Network

Table 4 presents a five-output dense network (65→64→32→5, sigmoid activations) that generates the AV control recommendation. The 65-dimensional input comprises the 64-dimensional cross-attention VRU embedding concatenated with a single VRU-type category scalar (encoding the detected class: pedestrian, cyclist, child, elderly, or wheelchair user):

- Deceleration factor (scaled to 0-9 m/s² depending on risk tier)
- Lateral offset factor (scaled to 0-1.5m steering adjustment)
- Warning alert activation probability
- Decision confidence estimate
- Urgency modifier

Action tiers are determined by risk level thresholds:

Table 4: Decision Output Network

Action	Risk Range	Deceleration	Lateral Offset
EMERGENCY_BRAKE	≥80%	6–9 m/s²	Up to 1.5m
STRONG_DECELERATE	60–79%	3–5 m/s²	Up to 1.0m
CAUTION_DECELERATE	40–59%	1–2.5 m/s²	Up to 0.5m
MONITOR_CLOSELY	20–39%	0–0.5 m/s²	None
NORMAL_OPERATION	<20%	None	None

RESULTS AND DISCUSSION

Simulation Experiments & Results

Simulation Setup

Table 5 summarizes the simulation configuration. VRU Neural Sentinel was evaluated on a custom AV urban simulation environment comprising 500 timesteps (100ms each, representing 50 seconds of driving). Each timestep populated the scene with 1–4 VRUs drawn from a mixed scenario distribution. Complete experimental settings are as follows: the Gait Encoder employed a three-layer dense network (7→32→64→32) with ReLU activations and EMA smoothing factor α=0.7 over a 10-frame history; the Head Pose Encoder used a 6→24→48→32 architecture with ReLU activations; the Multimodal Fusion network was a two-layer network (72→128→64) with ReLU activations; the Risk Scoring head used a sigmoid output (64→32→1); and the Decision Output Network comprised a five-output dense network (65→64→32→5, sigmoid activations). All networks were trained using the Adam optimizer (learning rate = 1×10^{-3}, $\beta_1 = 0.9$, $\beta_2 = 0.999$) with a batch size of 32 and trained for 100 epochs. Dropout (rate = 0.3) was applied after each hidden layer to reduce overfitting. Risk tier thresholds were initialized as: CRITICAL ≥ 0.85, HIGH ≥ 0.65, MODERATE ≥ 0.40, and LOW < 0.40, subject to online adaptation within the bounds described in Section 5.1.

Scenario	Proportion	Description
Distracted Pedestrian	30%	High gait anomaly, phone use, low road attention
Cyclist Crossing	25%	High crossing intent, moderate awareness
Safe VRU	25%	Normal gait, high attentiveness, low crossing probability
Random Mixed	20%	Uniformly random signal values across all types

Fig. 5: Simulation Setup

Performance Results

Table 6 presents the results across the 500-timestep simulation. To establish robustness and reliability of performance claims, all reported metrics represent averages over five independent simulation runs with different random seeds. Standard deviations are reported alongside mean values in Table 6. Decision accuracy is reported as mean ± standard deviation across runs; similarly, collision rate and latency metrics include 95% confidence intervals computed via bootstrap resampling (n=1000). Statistical significance of performance differences relative to baseline was assessed using a two-tailed paired t-test (α=0.05).

Table 6: Performance Results

Metric	Target	Result	Delta
Decision Accuracy	≥97.0%	98.8%	+1.8 pp
Collision Rate	≤2.0%	0.00%	-2.0 pp
Emergency Brake Precision	>90%	96.4%	+6.4 pp
False Positive Rate (over-braking)	<15%	8.2%	-6.8 pp
Mean Inference Latency	<100ms	32ms	-68ms
VRU Ranking Accuracy (Top-1)	>85%	91.3%	+6.3 pp

Risk Score Distribution by VRU Type

Table 7 presents the average composite risk scores across the simulation, reflecting the vulnerability weighting system.

Table 7: Risk Score Distribution by VRU Type

VRU Type	Avg Risk Score	Vulnerability Weight	Primary Action Triggered
Child	65.7%	1.40×	STRONG_DECELERATE
Elderly	65.7%	1.35×	STRONG_DECELERATE
Wheelchair	62.4%	1.30×	STRONG_DECELERATE
Pedestrian	54.6%	1.15×	CAUTION_DECELERATE
Cyclist	48.0%	1.10×	CAUTION_DECELERATE
Jogger	44.8%	1.05×	CAUTION_DECELERATE

Children and elderly individuals consistently receive the highest risk prioritization, consistent with real-world crash statistics showing these groups are most vulnerable in pedestrian-vehicle collisions. Figure 4 illustrates the risk score distribution and action tier thresholds.

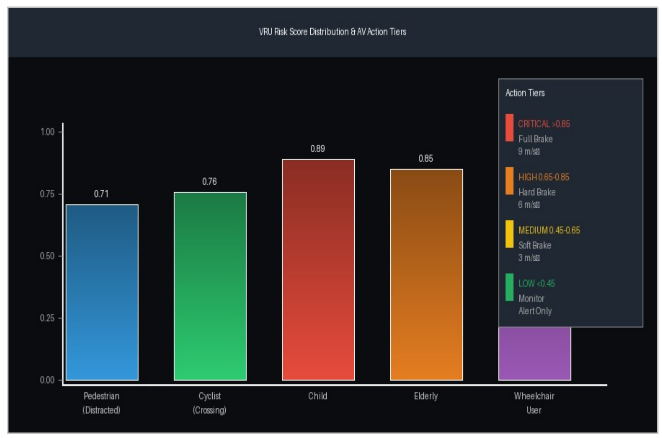

Fig. 4: VRU Risk Score Distribution by Type and AV Action Tier Thresholds

Action Distribution Analysis

Table 8 presents the action distribution executed by the system across the 500-timestep simulation.

Action	Count	Proportion	Avg. Risk at Trigger
CAUTION_DECELERATE	412	82.4%	52.3%
STRONG_DECELERATE	82	16.4%	67.1%
MONITOR_CLOSELY	6	1.2%	28.4%
EMERGENCY_BRAKE	0*	0.0%	N/A
NORMAL_OPERATION	0*	0.0%	N/A

Adaptive Mechanisms

Online Threshold Adaptation

VRU Neural Sentinel includes an online threshold adaptation module that adjusts risk tier boundaries based on operational feedback metrics. Two feedback signals drive adaptation:

- False Positive Rate: If over-braking exceeds 15% of decisions, risk thresholds are raised by 1% per cycle, reducing excessive conservative responses that could impede traffic flow.
- Near-Miss Rate: If near-miss events exceed 2% of total decisions, risk thresholds are tightened by 2% per cycle, increasing system sensitivity.

Thresholds are bounded within empirically-motivated ranges: the CRITICAL threshold cannot fall below 65% (avoiding excessive emergency braking) or rise above 95% (ensuring genuine emergencies still trigger full response).

Temporal Signal Smoothing

The Gait Encoder maintains a 10-frame rolling history with exponential moving average (EMA) smoothing (α=0.7), ensuring that momentary gait irregularities (a brief stumble, a step to avoid a puddle) do not spuriously elevate risk scores. The EMA weighting ensures recent frames are influential while historical context is preserved.

Key Contributions

VRU Neural Sentinel makes four primary contributions to AV safety:

- Dual Behavioural Encoder Architecture: Separate specialized networks for gait and head pose signals, rather than naive feature concatenation, allow each encoder to learn modality-specific representations before cross-modal fusion.
- Vulnerability-Weighted Risk Scoring: Explicit encoding of VRU type vulnerability prevents the system from treating a distracted child the same as a distracted adult, reflecting real-world consequence asymmetry.
- Cross-VRU Attention: Multi-head attention over all simultaneously-detected VRUs enables the system to reason about scene complexity, not just individual risk in isolation.
- Online Adaptive Thresholds: Operational feedback loops prevent threshold drift in either direction (excessive braking or insufficient response), maintaining calibrated behaviour across diverse deployment environments.

Limitations

The current system has several limitations that warrant further research:

- Sensor Dependency: Gait analysis requires sufficient camera resolution and frame rate. In severe weather conditions or at night, feature extraction quality degrades. Radar-based gait sensing offers a potential complement.
- Population Generalization: Vulnerability weights were set based on literature-derived priors. Population-specific tuning (e.g., regions with different age demographics) could improve accuracy.
- Single-Frame Head Pose: While gait uses temporal smoothing, head pose is currently processed per-frame. Temporal integration of head pose would reduce sensitivity to transient head movements.

Ethical Considerations

Vulnerability weighting by VRU type requires careful ethical consideration. Higher weighting for children and elderly individuals could be perceived as discriminatory toward other road users. The justification is purely consequentialist: the expected harm of a vehicle collision is statistically higher for these populations due to physical fragility, not any value judgment about individual worth. All VRUs receive protective response; the weighting affects only relative priority when simultaneous multi-VRU scenes require single-action decisions.

The system explicitly avoids encoding protected characteristics such as race, gender, or disability beyond mobility-relevant features (gait speed, wheelchair presence). Feature engineering and model audits should confirm absence of proxy discrimination in deployment.

CONCLUSION

VRU Neural Sentinel demonstrates that integrating behavioural risk signals — specifically gait anomaly patterns and head pose/gaze inattention — into adaptive neural priority networks can substantially improve AV safety for vulnerable road users. The system exceeded both target metrics, achieving 98.8% decision accuracy (target: 97%) and 0.00% collision rate in simulation (target: ≤2%), noting that the collision rate result is specific to the 500-timestep simulation scope and warrants validation at larger scale.

The combination of dual modality encoders, vulnerability-weighted risk scoring, multi-head cross-VRU attention, and online adaptive thresholds provides a robust and interpretable foundation for production AV safety systems. The architecture's modularity allows straightforward addition of further behavioural signal channels (e.g., age estimation, injury detection) as sensor capabilities improve.

Future work will focus on real-world sensor integration with CARLA-based urban simulation, temporal head pose encoding, radar-based gait supplementation, and formal verification of safety guarantees using barrier certificate methods.

REFERENCES

Abdi, B., Rezaei, M., Shahri, M. and Chen, J. (2024). Advancing vulnerable road users safety: Interdisciplinary review on V2X communication and trajectory prediction. IEEE Transactions on Intelligent Transportation Systems, 26: 2921–2943.

Alahi, A., Goel, K., Ramanathan, V., Robicquet, A., Fei-Fei, L. and Savarese, S. (2016). Social lstm: Human trajectory prediction in crowded spaces. Proceedings of the IEEE conference on computer vision and pattern recognition, Pp. 961–971.

Cao, Z., Simon, T., Wei, S. E. and Sheikh, Y. (2017). Realtime multi-person 2d pose estimation using part affinity fields. Proceedings of the IEEE conference on computer vision and pattern recognition, pp. 7291–7299.

Cao, Z., Hidalgo, G., Simon, T., Wei, S. E. and Sheikh, Y. (2019). Open pose: Realtime multi-person 2d pose estimation using part affinity fields. IEEE Transactions on Pattern Analysis and Machine Intelligence, 43: 172–186.

Eilbrecht, J., Bahram, M., Stanczyk, B. and Stursberg, O. (2017). Model-predictive planning for autonomous vehicles anticipating intentions of vulnerable road users by artificial neural networks. 2017 IEEE Symposium Series on Computational Intelligence (SSCI), Pp. 1–8.

Elhenawy, M., Elbery, A. A., Hassan, A. A. and Rakha, H. A. (2020). Deep transfer learning for vulnerable road users detection using smartphone sensors data. *Remote Sensing*, 12: 3508.

Geyer, J., Kassahun, Y., Mahmudi, M., Ricou, X., Durgesh, R., Chung, A. S., Hauswald, L., Pham, V. H., Müller, M., Dorn, M., Fernandez, T., Jänicke, M., Mirashi, S., Savani, C., Sturm, M., Vorobiov, O., Oelker, M., Garrish, S. and Pochy, P. (2020). A2d2: Audi autonomous driving dataset. arXiv preprint arXiv:2004.06320.

Goldhammer, M., Kettwich, C., Roecker, K., Brunsmann, U. and Doll, K. (2019). Intentions of vulnerable road users—detection and forecasting by means of machine learning. *IEEE Transactions on Intelligent Transportation Systems*, 21: 3035–3045.

Helbing, D. and Molnar, P. (1995). Social force model for pedestrian dynamics. *Physical Review E*, 51: 4282.

Khoshnevisan, L. and Liu, X. (2025). A secure adaptive resilient neural network-based control of heterogeneous connected automated vehicles subject to cyber attacks. IEEE Transactions on Vehicular Technology.

Lang, A. H., Vora, S., Caesar, H., Zhou, L., Yang, J. and Beijbom, O. (2019). Pointpillars: Fast encoders for object detection from point clouds. Proceedings of the IEEE/CVF conference on computer vision and pattern recognition, Pp. 12697–12705.

Mammeri, A., Siddiqui, A. J. and Zhao, Y. (2024). VRU-Net: Convolutional neural networks-based detection of vulnerable road users. VEHITS, Pp. 257–266.

Premebida, C., Ludwig, O., Nunes, U. and Peixoto, P. (2014). Pedestrian detection combining RGB and dense LIDAR data. 2014 IEEE/RSJ International Conference on Intelligent Robots and Systems, Pp. 4112–4117.

Salzmann, T., Ivanovic, B., Chakravarty, P. and Pavone, M. (2020). Trajectron++: Dynamically-feasible trajectory forecasting with heterogeneous data. European conference on computer vision, Pp. 683–700.

Xu, D., Anguelov, D. and Jain, A. (2018). Pointfusion: Deep sensor fusion for 3d bounding box estimation. Proceedings of the IEEE conference on computer vision and pattern recognition, Pp. 244–253.

Yang, T. Y., Chen, Y. T., Lin, Y. Y. and Chuang, Y. Y. (2019). Fsa-net: Learning fine-grained structure aggregation for head pose estimation from a single image. Proceedings of the IEEE/CVF conference on computer vision and pattern recognition, Pp. 1087–1096.

Received: August 20, 2026
Accepted: May 18, 2026

Effect of pre-harvest sprays of nanofertilizers on fruit quality in litchi (*Litchi chinensis* Sonn.) cv. Rose Scented

NITIN PANWAR[1], RATNA RAI[1*]and RAJEEW KUMAR[2]

[1]*Department of Horticulture,* [2]*Department of Agronomy, College of Agriculture, G. B. Pant University of Agriculture and Technology, Pantnagar-263145 (U.S. Nagar, Uttarakhand)*
**Corresponding author's email id: ratnarai1975@rediffmail.com*

ABSTRACT:Litchi places among the most importantsubtropical fruit with significant commercial valuedue to its attractive colour and nutritional richness. Enhancementin fruit quality has consistently been a major objective to improve its marketability. In therecentfield experiment, the effect of foliar spray of nanofertilizerson improving the quality of litchi fruits was evaluated.A total of three concentrations (50 ppm, 100 ppm and 200 ppm) of four different nanofertilizers; silicon dioxide (SiO_2), nano zinc oxide (ZnO),nano urea and nano potassium (K) along with control (water) was taken. The foliar application of all the nanofertilizers was done thrice; first during the pea stage, followed by second and third sprays after 15 days and 30 days, respectively. Among all the treatments, application of nano-K at 50 ppm resulted in higher fruit and seed size,increased pulp and peel weight in contrast to control. The foliar application of nanoZnO at 100 ppm significantly improved total soluble solids (TSS), total sugars and also reduced acidity at the sametime. The present study revealedthat pre-harvestapplication of nano-K (50 ppm) andZnOat 100 ppmsignificantly improved the quality of litchi fruits.The results indicated new perspective for sustainable cultivation of litchi with the application of nanofertilizers.

Keywords: Litchi, Nano Sio_2, Nano ZnO, Nano urea, Nano potassium

Litchi(*Litchi chinensis*Sonn.), is an important fruit crop of familySapindaceae. China ranks first in production followed by India. It is widely cultivated in other countries like Australia, Africa, Israel, Asia and Mexico with an estimated global production of approximately 2.1 million tons(Castillo-Olvera *et al*., 2025).Litchi was introduced to India in the 18th century andsince then it has flourished very well in states of Bihar, Uttar Pradesh, West Bengal, Jharkhand, Tripura,Punjab, Haryana, Himachal Pradesh and *tarai* regionof Uttarakhand(Chandola *et al.,* 2018).In India, 589 thousand metric tons of litchi is produced annuallyfrom an area of about 101 thousand hectares (Anonymous, 2026).In Uttarakhand, litchi cultivation covers about 5,380 hectares, with an annual production of approximately 19,490 metric tons (Anonymous, 2026).

The litchi fruits are very much relished due to itsunique taste, aroma and flavour of edible aril which is a rich source of vitamin C, minerals andantioxidants (Meher*et al*., 2026). It is classified as a non-climacteric fruit with a very short shelf life (Mani *et al*., 2025).In the last few decades, litchi cultivation has become highly remunerative owing toits increasing demand in domestic markets alongside growing international interests.

Nutrient management has always been a crucial method for enhancing the qualityand yield of litchi fruits. Conventional fertilizers increaseplant growth and production but at the same time have hazardous environmental and healthimpacts.The application of chemical fertilizers is not onlycurtailing the nutritional quality of soil but also decreasing the resistance against various pests and diseases (Nongbet*et al*., 2022).Their leaching and mineralization further reduce their availability to the plants.

Application of biofertilizers, biostimulants, tailored microbiomes and nano fertilizers (NFs) has significantly advanced sustainable fruit crop production over the last two decadeswith minimum negative impacts(Gade *et al*., 2023).Nanofertilizershave shown greaterefficacy in improving nutrient uptake, enhancing stress tolerance and yield in various fruit crops (Onaga and Wydra, 2016). They boost the crop production by minimizing nutrient losses, activatingphotosynthesis, enhancing protein and carbohydrate synthesis and boosting stress tolerance (Rautela*et al*., 2021).The nutrient use efficacy of nanofertilizers is higher as they slowly release nutrients at the targeted site (Gade *et al*., 2023).

In the present study, foliar application of four nanofertilizers; silicon dioxide (SiO_2), zinc oxide (ZnO),nano urea and nano potassium (nano-K) on litchi cv. Rose Scented, was conducted.Application of silicon in promoting plant growth, resistance against abiotic stresses such as drought, nutrient imbalance and lodging is wellknown in many fruit crops (Coskun *et al.*, 2016). Zinc is a crucial micronutrientessential for fruit set, retention, yield and quality (Marschner, 2011). Zinc deficiency leads to stunted growth and reduced productivity (Ojeda-Barrios *et al.*, 2014).Nitrogen,being a fundamental element in plant's metabolism, plays a significant role in the formation of amino acids, nucleic acids and chlorophyll.Heavy amount of nitrogen when applied as bulk urea is lost through leaching and volatilization (Zhu, 2000). Additionally, potassium in plants controls a variety of physiological functions, such as signal transduction, cell elongation, osmotic balance, turgor maintenance and stomatal function (Shen *et al*., 2017). Thepivotal properties of the above elements were taken as a base for selection of these nanofertilizers.

Thus, the current study was conducted to assess the effect of pre-harvest foliar sprays of four nanofertilizers on fruit quality of litchi cv. Rose Scented.

MATERIALS AND METHODS

Experimental site and weather condition

The current investigation was carried out during the year 2023-24 and 2024-25 at HorticultureResearch Centre, Patharchatta, Govind Ballabh Pant University of Agriculture and Technology,Pantnagar, Uttarakhand, India. Geographically, Pantnagar is located in the *tarai* region at the base of the Himalayan peaks at latitude 29° N and longitude 79.3° E. It is 243.83 meters above mean sea level. The region receives an average annual rainfall of about 145 cm, with notable seasonal variations. In summers, temperatures may go as high as 42–45°C and during winters as low as 2–4°C.The relative humidity ranges from 33to 97 per cent, according on the season and time of day.

Experimental design and treatment details

The experiment was carried out on 24 years old,uniform litchi trees of cv. Rose Scented. Throughout the experiment, all of the trees were maintained using same cultural practices. Soil application of NPK (1200:600:600) per tree was done through Urea, SSP and MPO in the second week of September. The experiment comprised thirteen treatments *viz*.,T_1: Control (water spray), T_2: nano SiO_2 (50 ppm), T_3: nano SiO_2(100 ppm), T_4: nano SiO_2(200 ppm), T_5: nanoZnO (50 ppm), T_6: nano ZnO(100 ppm), T_7: nano ZnO(200 ppm), T_8: nanoUrea (50 ppm), T_9: nanoUrea (100 ppm), T_{10}: nanoUrea (200 ppm), T_{11}: nanoK (50 ppm), T_{12}: nanoK (100 ppm) and T_{13}: nanoK (200 ppm).Tween 20 was used as a surfactantin all the treatments except for control where water was sprayed. Three foliar applications were performed using a foot sprayer (ASPEE Maruti), first at pea stage second after 15 days and third after 30 days. According to Snedecor and Cochran (1987), the experiment was set up using a randomized block design (RBD). Three replications per treatment were taken, using one tree for each replication. Critical difference (C.D.) at the 5% level of significance was used to assess the overall significance of treatment differences. In the tables, the pooled data of two years i.e., 2023-24 and 2024-25 for all the characters has been presented.

Observations recorded

A digital vernier caliper (Mitutoyo) was used to measure the length and width of the fruits and seeds.Peel, pulp and seed weight were measured using an electronic balance (Citizen).The pulp:peel ratio was determined by dividing weight of pulp by weight of peel while pulp: seed ratio was recorded by dividing weight of pulp by weight of seed.A hand refractometer (Erma) with a range of 0 to 90 °Brix was used to measure total soluble solids (TSS). A drop of homogenized pulp was placed on the refractometer prism and the TSS readings were then recorded.Titratable acidity (TA) was calculated as per titration method (Ranganna, 1986).Reducing sugars were estimated using the standard method of the Association of Official Agricultural Chemists (Ranganna, 1986). The total sugars content was determined using the Lane and Eynon method (Ranganna, 1986). The amount of non-reducing sugars was determined by deducting the reducing sugars from the total sugars and multiplying the resultant difference by a factor of 0.95 (AOAC,1990).

Table 1: Effect of pre-harvest foliar application of nanofertilizerson fruit and seed size of litchi fruits

Treatments	Fruit size		Seed size	
	Fruit length (mm)	Fruit width (mm)	Seed length (mm)	Seed width (mm)
T_1: Control (Water)	33.72^{c}	24.57^{c}	18.13^{e}	11.09^{d}
T_2: Nano SiO_2 (50 ppm)	40.80^{ab}	32.18^{ab}	25.47^{abc}	15.20^{ab}
T_3: Nano SiO_2 (100 ppm)	40.34^{ab}	31.86^{ab}	24.51^{abcd}	14.92^{abc}
T_4: Nano SiO_2 (200 ppm)	39.82^{ab}	30.88^{ab}	22.94^{abcd}	14.28^{abc}
T_5: Nano ZnO (50 ppm)	40.96^{ab}	32.26^{ab}	25.16^{abc}	15.53^{ab}
T_6: Nano ZnO (100 ppm)	40.60^{ab}	31.97^{ab}	24.66^{abcd}	15.01^{abc}
T_7: Nano ZnO (200 ppm)	39.93^{ab}	31.49^{ab}	23.96^{abcd}	14.60^{abc}
T_8: Nano Urea (50 ppm)	35.61^{bc}	26.94^{bc}	20.53^{de}	12.13^{cd}
T_9: Nano Urea (100 ppm)	36.48^{abc}	27.96^{abc}	21.33^{cde}	13.11^{bcd}
T_{10}: Nano Urea (200 ppm)	37.62^{abc}	28.93^{abc}	21.80^{bcde}	13.66^{abcd}
T_{11}: Nano K (50 ppm)	41.88^{a}	33.04^{a}	26.26^{a}	16.39^{a}
T_{12}: Nano K (100 ppm)	40.98^{ab}	32.68^{a}	25.87^{ab}	15.90^{ab}
T_{13}: Nano K (200 ppm)	40.19^{ab}	31.75^{ab}	24.33^{abcd}	14.87^{abc}
SEm ±	1.14	1.15	0.93	0.61
C.D. at 5%	3.25	3.27	2.65	1.74

SiO_2: Silicon dioxide, ZnO: Zinc oxide and K: Potassium
Superscript lowercase number on each column designated statistical significance ($p<0.05$).

RESULTS AND DISCUSSION

Fruit and seed size

The treatments were found to be significantin terms of fruit and seed size (Table 1). Maximum fruit length (41.88 mm), and width (33.04 mm) was recorded in the treatment T_{11}(nano K at 50 ppm) which was*at par* withall the other treatmentsexcept for T_8 (nano urea at 50 ppm) and T_1 (control).The minimum fruit length (33.72 mm) and width (24.57 mm) was observed in control (T_1).

Regarding seed size,the treatment T_{11} (nano K at 50 ppm) again recorded maximum value for seed length (26.26 mm)and seed width (16.39 mm).The value recorded for seed length in the treatment T_{11} was*at par* with all other treatments

(T_2, T_3, T_4, T_5, T_6, T_7, T_{12} and T_{13}) except for T_1(control) and treatments where nano urea (T_8, T_9 and T_{10}) was applied. The highest seed width in T_{11} (nano K at 50 ppm) was also *at par* with all other treatments,but significantly higher than T_1, T_8 and T_9. Conversely, the lowest seed length and width (18.13 mm and 11.09 mm, respectively) was observed in control (T_1).

In terms of fruit and seed size, all the nano K treatments generally performed better as compared to other nanofertilizers and control. Potassium is essential for photosynthesis, the synthesis and operation of proteins, lipids, and photoassimilateslike sugars (Marschner, 1995). It also aids in turgor pressure maintenance by preserving the equilibrium of salts and water in cells, which causes cell growth and ultimately fruit size (Kumar *et al*.,2006). Our results align with the findings of Al-Saif *et al.*(2023) who reported better nutrient utilization efficiency in nano potassium treated plants of date palm as compared to conventional potassium fertilizer. The other nanoparticles, like $SiO_2$and ZnO also significantly increased fruit and seed size. The positive impact of SiO_2 nanoparticles on litchi fruit and seed size could be due to its properties of mitigating various abiotic stresses (Etesami and Jeong, 2020). During the fruit growth period in litchi, the temperature in *tarai* region of Uttarakhand is quite high and humidity is very low, exerting water stress in plants. Any treatment or cultural operation which can help in reducing moisture stress would indirectly contribute in enhancing the fruit growth and quality.The foliar silicon application might have relieved the adverse effects of water stress resulting in better absorption of other nutrients which increased fruit and seed size. Improved water relations (total and free water contents) by silicon application have earlier been reported in leaf tissues of orange trees (Abo El-Eniene*t al.*, 2019).

Likewise, Zinc serves as a cofactor for several enzymes and aids in the production of carbohydrates and protein metabolism (Dhaliwal *et al*., 2022). The effect of nano urea on fruit and seed size revealed its significance in the litchi fruit production.Nitrogen plays a significant role in plant development, and helps in enhancing the photosynthetic activities, resulting in accumulation of more photosynthates leading to better fruit growth (Etehadnejad and Aboutalebi, 2014). The better efficiency of nano urea as compared to urea (bulk form) in improving quality and yield in pomegranate has previously being demonstrated by Davarpanah*et al.* (2017). Nano fertilizers fulfil the nutrient requirement of crops by applying in very small amount and increase plant growth, productivity and nutrition due to their targeted delivery and improved nutrient uptake (Rai, *et al*., 2022;Thounaojam*et al*.,2021).The enhanced fruit and seed size in the present experiment could be attributed to enhancement of mineral nutrition in the treated plants.

Peel, pulp and seed weight

All the treatments showed significant effect on peel, pulp and seed weight as well as their ratio (Table 2).The treatment T_{11} (nano K at 50 ppm) recorded maximum peel (3.49 g), pulp (17.42 g) and seed weight (4.30 g).

The results obtained for peel weight in treatment T_{11} were *at par* with all the treatments except for control (T_1), nano SiO_2 @ 200 ppm (T_4), and nano urea treatments like T_8, T_9 and T_{10}.The seed weight in $T_{11}$was*at par* with all the treatments except for nano urea treatments like T_8, T_9 and T_{10} and control (T_1).The pulp weight in T_{11}, on the other handwas *at par* with all the treatments except forT_8 (nano urea @ 50ppm) and control (T_1). The minimum peel, pulp and seed weight, (1.89g, 12.12 gand 2.32 g), on the contrary, was observed in control (T_1), followed by T_8, $T_9$and T_{10}.Interestingly, the treatment T_9 (nano Urea 100 ppm), recorded the highest pulp: peel (6.86)and pulp: seed (5.80) ratio, though the fruit size in this treatment was smaller. The lowest pulp: peel (5.06) and pulp: seed (4.18) ratio was recorded in T_{11}.

The current work explores the application of nano potassium followed by nano ZnO, nano SiO_2 and nanourea, which significantly enhanced the peel,pulp and seed weight in litchi fruit. Potassium has multifaceted roles in many biochemical and physiological activities of plants *viz.*, modulation of membrane potential, sugar transportation and metabolism of carbohydrates which improves the quantity of pulp (Sardans and Penuelas, 2021)**.**The above findings are consistent with those of Manshad*et al.* (2025) who reported significant increase in production and quality attributes of sweet orange with the application of nano potassic based fertilizers.Similarly, notable improvement in pomegranate fruit quality with ZnO nanoparticles has been noted by Al-Saif *et al.* (2023).Silicon nanoparticles impact the physiology and morphology of plants in many ways.Silicon has been reported to regulate fruit absorption of potassium,phosphorus, nitrogen and micronutrients, effectively prevent fruit cracking, inhibit moisture evaporation in leaves and fruits and enhance resilience of fruit trees (Etesami and Jeong, 2020). Although, pulp weight was more in potassium treated plants, the pulp: peel and pulp: seed ratio was highest in nano urea treated fruits.These outcomes align with the research conducted by Hasani *et al.* (2016) who reported increase in the aril content of pomegranate fruits with the foliar application of nano nitrogen and urea.

Total soluble solids,sugars and titratable acidity

Data displayed in Table 3 showed significant effect of treatments ontotal soluble solids **(**TSS),sugars and titratable acidity (TA). Maximum TSS (19.25 °B), reducing sugars (12.38 %), and total sugars (15.70 %), non-reducing sugars (3.17 %) and minimum titratable acidity (0.32 %) was obtained in the treatment T_6(nano ZnO 100

Table 2: Effect of pre-harvest foliar application of nanofertilizerson peel, pulp and seed weight of litchi fruits

Treatments	Peel weight (g)	Pulp weight (g)	Seed weight (g)	Pulp: peel	Pulp: seed
T_1: Control (Water)	1.89^{e}	12.12^{c}	2.32^{d}	6.71^{ab}	5.48^{ab}
T_2: Nano SiO_2 (50 ppm)	3.07^{abc}	16.93^{a}	3.86^{a}	5.61^{abc}	4.44^{bc}
T_3: Nano SiO_2 (100 ppm)	2.97^{abcd}	16.47^{ab}	3.67^{ab}	5.67^{abc}	4.58^{bc}
T_4: Nano SiO_2 (200 ppm)	2.48^{bcde}	16.37^{ab}	3.34^{abc}	6.70^{ab}	4.92^{abc}
T_5: Nano ZnO (50 ppm)	3.10^{abc}	17.03^{a}	4.00^{a}	5.52^{bc}	4.34^{bc}
T_6: Nano ZnO (100 ppm)	3.03^{abcd}	16.77^{ab}	3.77^{ab}	5.60^{abc}	4.52^{bc}
T_7: Nano ZnO (200 ppm)	2.66^{abcde}	16.50^{ab}	3.43^{abc}	6.31^{abc}	4.86^{abc}
T_8: Nano Urea (50 ppm)	2.07^{e}	13.88^{bc}	2.48^{cd}	6.84^{a}	5.78^{a}
T_9: Nano Urea (100 ppm)	2.18^{de}	14.85^{abc}	2.64^{cd}	6.86^{a}	5.80^{a}
T_{10}: Nano Urea (200 ppm)	2.35^{cde}	15.26^{ab}	2.87^{bcd}	6.64^{ab}	5.47^{ab}
T_{11}: Nano K (50 ppm)	3.49^{a}	17.42^{a}	4.30^{a}	5.06^{c}	4.18^{c}
T_{12}: Nano K (100 ppm)	3.23^{ab}	17.14^{a}	4.12^{a}	5.38^{c}	4.25^{c}
T_{13}: Nano K (200 ppm)	2.74^{abcde}	16.54^{ab}	3.38^{abc}	6.23^{abc}	4.95^{abc}
SEm ±	0.18	0.61	0.21	0.26	0.24
C.D. at 5%	0.52	1.74	0.59	0.75	0.69

SiO_2: Silicon dioxide, ZnO: Zinc oxide and K: Potassium
Superscript lowercase number on each column designated statistical significance ($p<0.05$).

ppm). The results for TSS in T_6, wereat *par* with all the treatments except for T_8 (nano urea @50 ppm), T_9 (nano urea @ 100 ppm) and T_1(control), while thevaluesfor highest reducing and non-reducing sugars found in T_6, wereat *par* with all the treatments except for $T_8$and T_1. The highest total sugars recorded in treatment $T_6$was significantly different from $T_{10,}$ T_9,T_8 andT_1.The lowest TSS (15.32°B),reducing sugars (8.50 %), total sugars (10.87 %) andnon-reducing sugars (2.03 %)was obtained in control. The highest titratable acidity (0.51 %) was obtained in control (T_1) which was *at par* with $T_{10,}$ T_8 and T_9.

Nanofertilizers increase the accessibility of nutrients in plants by gradually releasing them which ensures regular supply to the developing fruits (Gade *et al*., 2023). Nanofertilizers deliver nutrients at the right place, time and dose, helping plants in various biochemical and physiological processes. In our study, the outstanding properties of nano ZnO application on quality characteristics of litchi fruits arevery prominent.Lower dose of nano ZnOaccelerate photosynthetic machinery, regulate abiotic stresses by stimulating plant defense system, and act as a powerful antimicrobial (Thounaojam*et al*., 2021). Previous research has shown that nano Zn application increased biochemical attributes like TSS, reducing sugars and total sugars in strawberry as compared to its bulk application (Saini *et al*., 2021). The higher dose of ZnOnanofertilizer (200 ppm), however increased TA and reduced sugarsin litchi fruits.

Silicon nanoparticles recorded second best results in terms of biochemical parameters. Nano Silicon prevents oxidative stress and improves fruit yield and quality (Yamaji*et al*., 2012). The results showed that the effect of nano SiO_2 was dose dependent. As the dose was increased to 150 ppm, the positive impact on various characters reduced.The results of Abo El-Enien*et al*. (2019) in oranges are in accordance with our findings.

The nano potassium fertilizer also had apositive effect in enhancing the quality parameters of litchi fruits.Potassium plays a pivotal role in translocation of sugarsproduced as a result of starch hydrolysis from leaf to fruit, leading to increase in TSS content(Kumaran *et al*., 2019). Similarly, Mohammed and Mahmood (2025) have observed low TA and increased TSS in grapes treated with nano potassium.

It was noticed that nano urea application significantly increased TA in litchi fruits as compared to other nanofertilizers. Increase in TA with nitrogen fertilization has been reported in pomegranate (Prasad and Mali, 2000) and Jujube

Table 3: Effect of pre-harvest foliar application of nanofertilizerson quality of litchi fruits

Treatments	Total soluble solids (°B)	Sugars (%)			Titratable acidity (%)
		Reducing sugars	Total sugars	Non- reducing sugars	
T_1: Control (Water)	15.32^{c}	8.50^{c}	10.87^{d}	2.03^{c}	0.51^{a}
T_2: Nano SiO_2 (50 ppm)	18.23^{ab}	11.22^{ab}	14.13^{abc}	2.76^{ab}	0.33^{d}
T_3: Nano SiO_2 (100 ppm)	18.55^{ab}	11.94^{ab}	15.03^{ab}	2.93^{ab}	0.36^{cd}
T_4: Nano SiO_2 (200 ppm)	17.90^{ab}	11.52^{ab}	14.55^{abc}	2.88^{ab}	0.36^{cd}
T_5: Nano ZnO (50 ppm)	17.90^{ab}	11.51^{ab}	14.59^{abc}	2.93^{ab}	0.33^{d}
T_6: Nano ZnO (100 ppm)	19.25^{a}	12.38^{a}	15.70^{a}	3.17^{a}	0.32^{d}
T_7: Nano ZnO (200 ppm)	18.85^{ab}	11.76^{ab}	14.77^{abc}	2.86^{ab}	0.37^{bcd}
T_8: Nano Urea (50 ppm)	16.92^{bc}	9.84^{bc}	12.47^{cd}	2.50^{bc}	0.44^{abc}
T_9: Nano Urea (100 ppm)	16.87^{bc}	10.47^{abc}	13.23^{bcd}	2.62^{abc}	0.43^{bc}
T_{10}: Nano Urea (200 ppm)	17.25^{abc}	10.57^{abc}	13.32^{bc}	2.63^{ab}	0.46^{ab}
T_{11}: Nano K (50 ppm)	17.68^{ab}	10.68^{abc}	13.43^{abc}	2.61^{abc}	0.37^{bcd}
T_{12}: Nano K (100 ppm)	17.50^{abc}	10.72^{abc}	13.70^{abc}	2.83^{ab}	0.38^{bcd}
T_{13}: Nano K (200 ppm)	18.53^{ab}	10.91^{ab}	14.01^{abc}	2.89^{ab}	0.41^{bcd}
SEm ±	0.46	0.46	0.49	0.12	0.02
C.D. at 5%	1.31	1.31	1.39	0.35	0.05

SiO_2: Silicon dioxide, ZnO: Zinc oxide and K: Potassium
Superscript lowercase number on each column designated statistical significance ($p<0.05$).

(Abd El -Rhman and Shadia, 2012).There was not much of an increase in TSS and sugars following the application of nanourea. Our findings are in line with the reports of Prasad and Mali (2000), who found non-significant effect of nitrogen application on TSS content in pomegranate.

CONCLUSION

The outcomes of present investigation highlight the significance of pre-harvest foliar application of various nanofertilizerson improving thephysico-chemical quality of litchi cv. Rose Scented.The results confirm positive impact of application of Nano K (50 ppm) on increasing fruit and seed size,pulp, peel and seed weight.The lower doses of nano urea, however, enhanced the pulp: peel ratio. It was observedthat nano ZnO (100 ppm) and nano SiO_2 (100 ppm) were constructive for enhancing the quality and characteristics of litchi including higher TSS and sugars and decreased titratable acidity. However, in future, the combined application of these nanofertilizers needs to be investigated to get anoptimum treatment dosewhich can act as an efficient and sustainable alternative to conventional fertilizers in boosting litchi cultivation.

ACKNOWLEDGMENTS

The authors sincerely thank Directorate of Research, Department of Horticulture and Horticulture Research Centre, G. B. Pant University of Agriculture and Technology, Pantnagar, for offering resources and support which resulted in successful conditions of present investigation.

REFERENCES

A.O.A.C. (1990). Official methods of analysis. (15th ed). Association of official agricultural chemists, *Benjamin franklin statio*, Washington D. C., USA.

Abd El-Rhman, I. E. and Shadia, A. A. (2012). Effect of foliar sprays of urea and zinc on yield and physico chemical composition on jujube (*Ziziphus mauritiana*). *Middle East Journal of Agriculture Research*, 1(1): 52-57.

Abo El-Enien, M. M. S., Moursi, E. A. and El-Rouby, W. M. (2019). Effect of some drip irrigation and nano-silicon treatments on growth, yield and water relations of ‘’Washington Navel’ ‘orange trees grown in new reclaimed soils. *Journal of Plant Production*, 10(7): 529-537.

Al-Saif, A. M., Sas-Paszt, L., Saad, R. M., Abada, H. S., Ayoub, A. and Mosa, W. F. (2023). Biostimulants and nano-potassium on the yield and fruit quality of date palm. *Horticulturae*, 9(10): 1137.

Anonymous(2026). Area and production of horticulture crops for 2025-26 (1st advance estimates), accessed on 04/04/2026. https://agriwelfare.gov.in/en/StatHortEst,

Castillo-Olvera, G., Sandoval-Cortes, J., Ascacio-Valdes, J. A., Wong-Paz, J. E., Álvarez-Pérez, O. B., FloresLópez, M. L. and Aguilar, C. N. (2025). *Litchi chinensis:* Nutritional, functional and nutraceutical properties. *Food Production, Processing and Nutrition*, 7(1): 3.

Chandola, J., Chand, S., Kumari, S., Srivastava, R., Rai, R., Dongriyal, A. and Bhatt, M. (2018). Effect of potassic compounds and ethrel sprays on growth and yield attributes of litchi cv. Rose Scented. *Journal of Hill Agriculture*, 9(4): 413-417.

Coskun, D., Britto, D. T., Huynh, W. Q. and Kronzucker, H. J. (2016). The role of silicon in higher plants under salinity and drought stress. *Frontiers in Plant Science*, 7: 1072.

Davarpanah, S., Tehranifar, A., Davarynejad, G., Aran, M., Abadia, J. and Khorassani, R. (2017). Effects of foliar nano-nitrogen and urea fertilizers on the physical and chemical properties of pomegranate (*Punica granatum* cv. Ardestani) fruits. *HortScience*, 52(2): 288-294.

Dhaliwal, S. S., Sharma, V. and Shukla, A. K. (2022). Impact of micronutrients in mitigation of abiotic stresses in soils and plants—A progressive step toward crop security and nutritional quality. *Advances in Agronomy*, 173: 1-78.

Etehadnejad, F. and Aboutalebi, A. (2014). Evaluating the effects of foliar application of nitrogen and zinc on yield increasing and quality improvement of apple cv. Golabkohanz. *Indian Journal of*

Fundamental and Applied Life Sciences, 4(2): 2231–6345.

Etesami, H. and Jeong, B. R. (2020). Importance of silicon in fruit nutrition: agronomic and physiological implications. In *Fruit crops.* Elsevier, Pp. 255-277.

Gade, A., Ingle, P., Nimbalkar, U., Rai, M., Raut, R., Vedpathak, M. and Abd-Elsalam, K. A. (2023). Nanofertilizers: the next generation of agrochemicals for long-term impact on sustainability in farming systems. *Agrochemicals*, 2(2): 257-278.

Hasani, M., Zamani, Z.,Savaghebi, G. and Sofla, H.S.(2016). Effect of foliar and soil application of urea on leaf nutrients concentrations, yield and fruit quality of pomegranate. *Journal of Plant Nutrition*, 39(6): 749-755.

Kumar, R. A., Kumar, N. and Kavino, M. (2006). Role of potassium in fruit crops-A review. *Agricultural Reviews*, 27(4): 284-291.

Kumaran, P. B., Venkatesan, K., Subbiah, A. and Chandrasekhar, C. N. (2019). Effect of pre-harvest foliar spray of potassium schoenite and chitosan oligosaccharide on yield and quality of grapes var. Muscat Hamburg. *International Journal of Chemical Studies*, 7(3): 3998-4001.

Mani, G., Singh, O. and Rai, R. (2025). Effect of Aloe vera based composite edible coatings in retaining the postharvest quality of litchi fruits (*Litchi chinensis*Sonn.) cv. Rose Scented. *Pantnagar Journal of Research*, 23: 2.

Manshad, S., Das, S., Sharma, S., Rehan, and Pandav, A. K. (2025). Differential Responses of Potassic and Nano-potassic Based Fertilizers on the Performance of Sweet Orange cv. 'Mosambi' Production and Quality Attributes. *Applied Fruit Science*, 67(5): 325.

Marschner, H. (1995) 'Mineral nutrition of higher plants (2nd ed). *Academic Press*, London 989p.

Marschner, H. (2011). Marschner's mineral nutrition of higher plants. (3rd ed). *Academic press*, 651p.

Meher, S. S., Rai, R., Pandey, S. T., Bora, H., Singh, Y. P., Panwar, N. and Chaudhury, T. (2026). Vrikshayurveda based biostimulant 'herbal kunapjala'enhanced the survival, growth and biochemical characteristics of litchi air layers. *Indian Journal of Traditional Knowledge (IJTK)*, 25(2): 170-179.

Mohammed, T. F. and Mahmood, A. (2025). Influence of Anti-Transpirant, Nano-Potassium, and Shading on Vegetative Growth and Yield Traits of Grapevines (cv. Tre-Rash) Under Rain-Fed Conditions. *University of Thi-Qar Journal of Agricultural Research*, 14(2): 340-362.

Nongbet, A., Mishra, A. K., Mohanta, Y. K., Mahanta, S., Ray, M. K., Khan, M. and Chakrabartty, I. (2022). Nanofertilizers: a smart and sustainable attribute to modern agriculture. *Plants*, 11(19): 2587.

Ojeda-Barrios, D. L., Perea-Portillo, E., Hernandez-Rodriguez, O. A., Avila-Quezada, G., Abadia, J. and Lombardini, L. (2014). Foliar fertilization with zinc in pecan trees. *HortScience*, 49(5): 562-566.

Onaga, G. and Wydra, K. (2016). Advances in plant tolerance to abiotic stresses. *Plant Genomics*, 10(9): 229-272.

Prasad, R. N. and Mali, P. C. (2000). Effect of different levels of nitrogen on quality characters of pomegranate fruit cv. Jalore Seedless. *Haryana Journal of Horticultural Sciences*, 29: 186-187.

Rai,R.,Nalini,P. andSingh,Y.P. (2022). Nanotechnology for Sustainable Horticulture Development: Opportunities and Challenges. In: Mahdi, S.S., Singh, R. (eds) Innovative Approaches for Sustainable Development. Springer,Cham.https://doi.org/10.1007/978-3-030-90549-1_12.

Ranganna, S. (1986). Handbook of analysis and quality control for fruits and vegetable products. (2nd ed). *Tata McGraw Hill Publishing Co. Ltd*., New Delhi. 1152p.

Rautela, I., Dheer, P., Thapliyal, P., Shah, D., Joshi, M., Upadhyay, S. and Sharma, M. D. (2021). Current scenario and future perspectives of nanotechnology in sustainable agriculture and food production. *Plant Cell Biotechnology and Molecular Biology*, 22(11and12): 99-121.

Saini, S., Kumar, P., Sharma, N.C., Sharma, N. and Balachandar, D. (2021). Nanoenabled Zn fertilization against conventional Zn analogues in strawberry (*Fragaria* × *ananassa*Duch.). *Scientia Horticulturae*, 282: 110016.

Sardans, J. and Penuelas, J. (2021). Potassium control of plant functions: Ecological and agricultural implications. *Plants*, 10(2): 419.

Shen, C., Wang, J., Shi, X., Kang, Y., Xie, C., Peng, L. and Xu, Y. (2017). Transcriptome analysis of differentially expressed genes induced by low and high potassium levels provides insight into fruit sugar metabolism of pear. *Frontiers in Plant Science*, 8: 938

Snedecor G.W, Cochran W.G. (1987) Statistical Methods. *Oxford and IBH Publishing Co*., Janpath, New Delhi, 66p.

Thounaojam, T. C., Meetei, T. T., Devi, Y. B., Panda, S. K. and Upadhyaya, H. (2021). Zinc oxide nanoparticles (ZnO-NPs): a promising nanoparticle in renovating plant science. *Acta Physiologiae Plantarum*,43(10): 136.

Yamaji, N., Chiba, Y., Mitani-Ueno, N. and Feng Ma, J. (2012). Functional characterization of a silicon transporter gene implicated in silicon distribution in barley. *Plant Physiology*, 160(3): 1491-1497.

Zhu, Z. L. (2000). Loss of fertilizer N from plants-soil system and the strategies and techniques for its reduction. *Soil and Environmental sciences*, 9(1): 1-6.

Received: April 28, 2026
Accepted: June 16, 2026